



HAL
open science

Sedimentary hydrodynamics of a sandy bay under macrotidal conditions (Saire Bay, France)

Gwendoline Gregoire, Anne Murat, Yann Méar, Emmanuel Poizot, Marion Claire, Sandric Lesourd, Haize Thomas, Adenot Camille

► **To cite this version:**

Gwendoline Gregoire, Anne Murat, Yann Méar, Emmanuel Poizot, Marion Claire, et al.. Sedimentary hydrodynamics of a sandy bay under macrotidal conditions (Saire Bay, France). *Journal of Maps*, 2023, 19 (1), 10.1080/17445647.2023.2206584 . hal-04290112

HAL Id: hal-04290112

<https://hal.science/hal-04290112v1>

Submitted on 20 Nov 2023

HAL is a multi-disciplinary open access archive for the deposit and dissemination of scientific research documents, whether they are published or not. The documents may come from teaching and research institutions in France or abroad, or from public or private research centers.

L'archive ouverte pluridisciplinaire **HAL**, est destinée au dépôt et à la diffusion de documents scientifiques de niveau recherche, publiés ou non, émanant des établissements d'enseignement et de recherche français ou étrangers, des laboratoires publics ou privés.



Distributed under a Creative Commons Attribution - NonCommercial 4.0 International License



Sedimentary hydrodynamics of a sandy bay under macrotidal conditions (Saire Bay, France)

Gregoire Gwendoline, Murat Anne, Méar Yann, Poizot Emmanuel, Marion Claire, Lesourd Sandric, Haize Thomas & Adenot Camille

To cite this article: Gregoire Gwendoline, Murat Anne, Méar Yann, Poizot Emmanuel, Marion Claire, Lesourd Sandric, Haize Thomas & Adenot Camille (2023) Sedimentary hydrodynamics of a sandy bay under macrotidal conditions (Saire Bay, France), Journal of Maps, 19:1, 2206584, DOI: [10.1080/17445647.2023.2206584](https://doi.org/10.1080/17445647.2023.2206584)

To link to this article: <https://doi.org/10.1080/17445647.2023.2206584>



© 2023 The Author(s). Published by Informa UK Limited, trading as Taylor & Francis Group on behalf of Journal of Maps



View supplementary material [↗](#)



Published online: 15 May 2023.



Submit your article to this journal [↗](#)



Article views: 347




View related articles [↗](#)



View Crossmark data [↗](#)



Sedimentary hydrodynamics of a sandy bay under macrotidal conditions (Saire Bay, France)

Gregoire Gwendoline ^{a,b}, Murat Anne^{a,b}, Méar Yann^{a,b}, Poizot Emmanuel^{a,b}, Marion Claire^{a,b}, Lesourd Sandric^c, Haize Thomas^{a,b} and Adenot Camille^{a,b}

^aConservatoire National des Arts et Métiers, Intechmer, Cherbourg-en-Cotentin, France; ^bLaboratoire Universitaire des Sciences Appliquées de Cherbourg, Normandie Université, Cherbourg-en-Cotentin, France; ^cLaboratoire Morphodynamique Continentale et Côtière (M2C – UMR 6143), Normandie Université, Unicaen, Caen, France

ABSTRACT

Identified as one of the most vulnerable environment to the impacts of sea-level rise, the morphological and hydrological diversity of coastal areas complicates their study. To understand their evolution, it is essential to characterize their current morpho-sedimentary distributions and processes. Morphologic interpretation, from LiDAR data, coupled with grain-size and geochemical analyses of 200 samples, subsequently interpreted with statistical tools (PCA), allow us to determine the pattern of sedimentary transport of Saire Bay (Normandy, France). Even if the area is mainly dominated by tidal currents, the original morphology of Saire Bay highlights an uncommon complex circulation on a sandy tidal flat. Sedimentary land-sea exchanges, induced by tidal current, do not occur through the river Saire network in the north, but in south, along a less apparent secondary channel. Results provide an essential base to better understand the evolution of the coastline.

ARTICLE HISTORY

Received 29 November 2022
Revised 13 April 2023
Accepted 15 April 2023

KEYWORDS

Morphology; sedimentology; X-ray geochemistry; coastal vulnerability; hydrodynamic; English channel

1. Introduction

At the land-sea interface, coastal environments are weakened by sea-level rise reflected by increased marine flooding events and an intensification of coastal erosion (FitzGerald et al., 2008; IPCC, 2019, 2021). Densely populated (23% population live both within 100 km of the coast and within 100 m of altitude), coastal environments are at the heart of major socio-economic issues. It is therefore essential to study them carefully.

The morphological diversity of coastal environments (estuaries, deltas, cliff, or sandy coasts) complicates the study of their evolutionary responses (Isla et al., 2018; Day et al., 2016; Costa et al., 2019; Roulland et al., 2022; Audère & Robin, 2021; Castelle et al., 2015; Foteinis & Synolakis, 2015; Luijendijk et al., 2018; Williams, 2013). Estuary evolution depends on three main factors: (1) their morphology (Du et al., 2018), (2) the sedimentary stock available, and (3) the rate of sea-level rise (Allen, 2000; Tessier, 2012). Today, in response to sea-level rise, coastal systems are tending towards a ‘re-balancing’: the hydro-sedimentary processes are evolving, and sedimentary sources are diversifying. Thus, to understand the response of a studied system, it is necessary to characterize its hydro-sedimentary processes and inputs.

In this framework, the Saire Bay, located in Normandy (France), appears to be an ideal sector for

understanding the processes of evolution of an intertidal macrotidal domain. It is a large sandy intertidal flat of 4 km² incised by the Saire river to the north. Its coastal fringe is subject to frequent marine submersion events and records regular degradation of the dykes that border it (25 degradation phenomena have been recorded over the last century, DDTM, 2016). However, no hydro-sedimentary studies have been carried out in this sector. The aim of this study was to establish (1) the nature and morphology of the intertidal sediment cover, (2) sediment sources, and (3) the influence of hydrodynamic agents in the intertidal area. The study is based on morphologic LiDAR interpretation and the analysis of 200 surface sediment samples collected in June 2019. Results can provide a basis to establish comparison and input into numerical and geostatistical predictive models (Baux et al., 2022) of sedimentary prism evolution. It can be better understood the evolution of erosion and marine submersion hazards with respect to sea-level rise and its acceleration by 2050.

2. Study area

Located at the eastern part of the Cotentin peninsula in France, the Saire Bay faces the eastern English

CONTACT Gregoire Gwendoline  Gwendoline.gregoire@lecnam.net  Conservatoire National des Arts et Métiers, Intechmer, Cherbourg-en-Cotentin 50100, France; Laboratoire Universitaire des Sciences Appliquées de Cherbourg, Normandie Université, Cherbourg-en-Cotentin 50100, France
 Supplemental data for this article can be accessed online at <https://doi.org/10.1080/17445647.2023.2206584>.

© 2023 The Author(s). Published by Informa UK Limited, trading as Taylor & Francis Group on behalf of Journal of Maps. This is an Open Access article distributed under the terms of the Creative Commons Attribution-NonCommercial License (<http://creativecommons.org/licenses/by-nc/4.0/>), which permits unrestricted non-commercial use, distribution, and reproduction in any medium, provided the original work is properly cited. The terms on which this article has been published allow the posting of the Accepted Manuscript in a repository by the author(s) or with their consent.

Channel (Main map). It is surrounded by Saint-Vaast-La-Hougue and Réville coastal cities. It is bounded by the ‘*pointe de la Saire*’ to the north and a line connecting Saint-Vaast-La-Hougue harbour to Tatihou island in the south. Oyster farms extended over 1.2 km² across this intertidal environment since the early twentieth century, whereas a large sandy domain free of human activities occurs to the north, where the Saire channel is well developed up to its estuary (N-W) (Figure 1). The linear Saint-Vaast-la-Hougue coastline, oriented NNE-SSW, was artificialized as of the seventeenth century, to protect the continental wetlands. Dykes, called ‘*longue rive*’, are 2.9 km long (Leroux, 1897). The Réville coastline is a 2.2 km long nonlinear shoreline, oriented NW-SE, characterized by rocky points and small convex sandy bays. It was locally artificially modified during the twentieth century to protect private constructions.

2.1. Geology and sedimentology

Two types of rock outcrops are found: (1) Hercynian (300 Ma) Barfleur granite forming the ‘*pointe de la Saire*’, the Tatihou granitic base, and the islet of ‘*Ben-être*’ beacon, and (2) brioverian (540 Ma), metamorphized sedimentary rocks mainly localized between the sandy domain and the oyster farms (Figure 1, Main map) (Graindor & Wasserburg, 1962). Domain Tectonic is characterized by

deformation induced during granite establishment and affecting the brioverian grounds (Dissler, 1987; Gresselin, 1990). The littoral platform is oriented according to this deformation, with a schistosity of N120E and well-marked by the northern contact between two units revealed by the coastline. Saire Bay is formed from brioverian rocks (schists and sandstones), more vulnerable to erosion and alteration than the granite which forms positive relief outcrops (Main map). The Saire Bay is located between two major English Channel sedimentologic domains: (1) coarse sediment cover in the north contrasting with (2) the fine sediments of the Seine Bay (datashom.fr). At a smaller scale, Saire Bay sedimentology is not well documented and is generalized as sandy sediment (fine to medium) (Savini, 2021).

2.2. Hydrodynamics

The Saire, a coastal river 31 km long, rises at Mesnil-au-Val and flows to the sea between the cities of Réville and Saint-Vaast-la-Hougue. Here, a hydraulic gate functioning according to the tides is closed during floods and opened during the ebb. The Saire watershed covers an area of 122 km² on brioverian rocks. The mean flow rate is about 1.65 m³ s⁻¹ and can reach 24 m³ s⁻¹ during flood season (October to March). Tide cycles are semidiurnal, and the mean tidal range is about 4 m (macrotidal regime), and

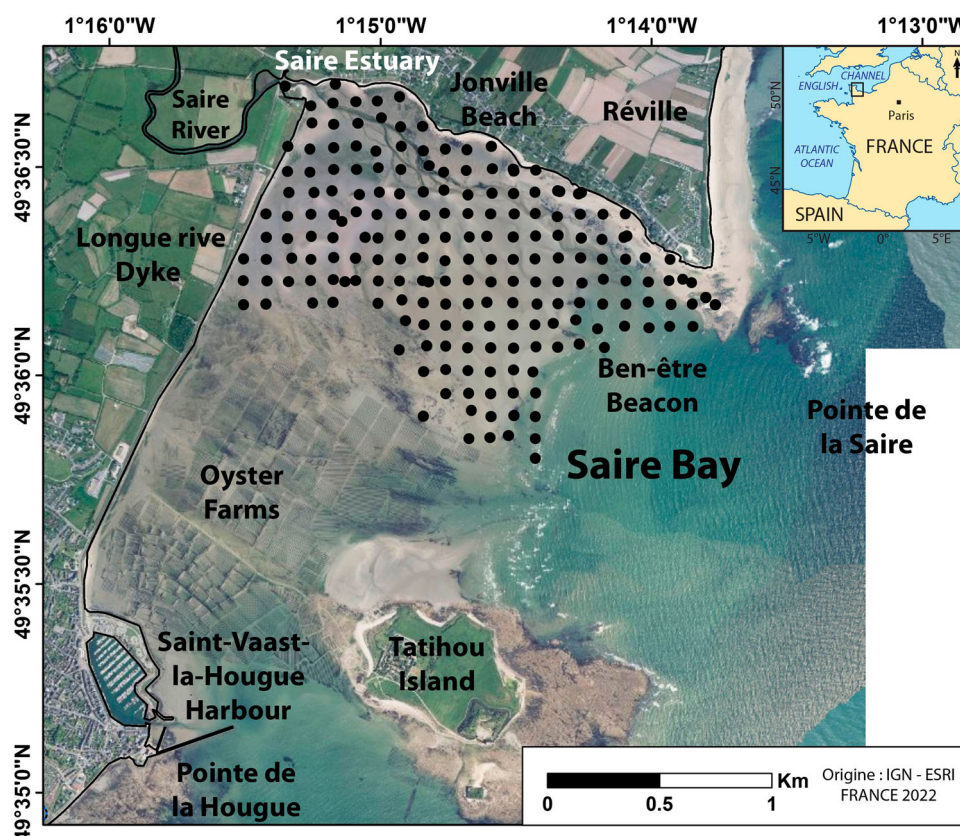


Figure 1. Study area and sample grid.

varies between a height of 7 and 1.5 m (SHOM, 1996). Stronger currents are located at the ‘*pointe de la Saire*’ and reach 1 m s^{-1} . The bay is characterized by currents lower than 0.5 m s^{-1} (Pommepuy et al., 2005). The study area is impacted by winds coming from two main directions.

The major wind direction (60% of the year) is between 200 and 240°N (SW). Mainly occurring in the winter, wind speeds are between 3.6 and 8.2 m s^{-1} during half part of winter and can exceed 13.9 m s^{-1} sporadically (10%). The second direction (30% of the year) is between 30 and 80°N (NE). Mainly occurring in the summer, wind speeds are mainly lowest (under 8.7 m s^{-1}) but can exceed 13.9 m s^{-1} in scattered events (Le Cam & Baraer, 2012). In extreme events, wind can exceed 27 m s^{-1} , such as during the Alex storm (2020/10/02), when gusts reached 36 m s^{-1} (Meteofrance.fr).

3. Methods

3.1. LiDAR data processing

LiDAR data were taken from the Litto3D Digital Elevation Model (DEM) (2016–2017) and distributed by ROL (Reseau d’Observatoire du Littoral Normandie – Haut de France) and SHOM (Service Hydrographique et Océanographique de la Marine) (<https://rolnp.fr>). This DEM (20 cm of vertical resolution), using the French altimeter system IGN69, was converted into Lowest Astronomical Tide (L.A.T). DEM analysis was performed using QGIS software. The analysis delimited (1) rocky outcrops, (2) sedimentary structures, and (3) anthropogenic installations (archaeological and contemporary) over 8.3 km^2 .

3.2. Sediment sampling

In total, 200 surface sediment samples were collected in June 2019 (medium spring tide). Stations form a grid spaced at 100 m (Figure 1). For each station, (1) coordinates were obtained through a GNSS instrument, (2) photographs were taken, and (3) surface sediments (1 cm depth) were collected over an area of 0.03 m^2 . We choose to focus our sampling on a flat sandy area localized between the north coastline

and the oyster farms, which we named ‘*central sandy tidal flat*’. In 2020, ten additional samples were collected on the watershed according to a similar protocol (Table 1).

3.3. Laboratory analyses

Grain size and geochemistry analyses of the sediment samples were performed following a rigorous protocol. This consisted of sub-sampling the raw samples to maintain one part at a temperature of 5°C and the second part at -18°C .

Grain size analyses were performed on the sub-samples maintained at 5°C. Sediment was mixed with 1.5 ml of sodium hexametaphosphate solution, agitated, submitted to ultrasounds for two minutes, and finally passed through a laser particle size analyzer (HORIBA LA-960). The LA-950v2 analyzed the grain size distribution by calculating the percentage size frequency of 96 classes over a size range of 0.011–3000 μm (error < 2%). Each sample was measured following the Mie theory (complex refractive index: Fluid RI: 1.33; Sample RI: 1.55; Imaginary RI: 0).

Frozen samples were lyophilized. The coarser fraction was removed with a 2-mm sieve. The finer part was ground into powder. The powders obtained were rinsed three times with purified water and then centrifuged. This step is carried out to eliminate the Br, I, and Cl contained in seawater and preserved in sediment during the lyophilization. Elemental contents were determined from an X-ray fluorescence spectrometry device (xSORT from Ametek). The xSORT allows both qualitative and quantitative measurements (by calibration) of different chemical elements (from Si for the lightest to U for the heaviest) to be obtained. Calibration was based on 45 marine samples previously analyzed by ICP-OES and ICP-MS methods.

3.4. Final map production

Final maps (Main map) were produced from the study of Principal Component Analysis (PCA) using the R language (R Core Team, 2016). The interpretation of the properties of the sub-populations is based on the

Table 1. Concentrations of four chemical elements used in geochemistry PCA, from sediments sampled in the Saire watershed (number 1–10) and their coordinates.

N#	Si (%)	Ca (%)	Sr (ppm)	Ti (ppm)	Mn (ppm)	X (°)	Y (°)
1	43.8	0.0	30	1580	230	1.25264°W	49.61226°N
2	45.6	0.0	21	1523	235	1.25405°W	49.61134°N
3	39.5	0.0	38	3035	1194	1.25273°W	49.61150°N
4	42.3	0.3	81	4313	843	1.25132°W	49.61160°N
5	39.4	0.2	69	4275	495	1.25000°W	49.61168°N
6	45.6	0.1	70	3477	400	1.24864°W	49.61190°N
7	45.9	0.1	76	4106	433	1.25394°W	49.61066°N
8	42.8	0.3	81	3969	847	1.25262°W	49.61065°N
9	44.3	0.2	89	3712	665	1.25112°W	49.61074°N
10	30.0	10.9	304	1039	200	1.24969°W	49.61101°N

calculated eigenvectors and relative weighting of the scalar quantities of eigenvalues. Interpolation maps (Main map) were produced from QGIS software.

4. Results and interpretation

4.1. Geomorphology

The study area is characterized by a complex variety of rocky platforms and a sandy tidal flat. It is cut by fluvial (Saire channel) and tidal networks where terraces and tidal bars are well developed, and shaped in complex sedimentary marine and intertidal structures, such as sandy prisms, banks, or marine dunes (Davis & Balson, 1992; Dyer & Huntley, 1999; Le Bot, 2001; Garlan, 2007; Neill et al., 2009; Garlan et al., 2015).

4.1.1. General morphological context

Granite platforms are well represented and cover an area of 0.5 km². They are mainly developed in proximity to the ‘*pointe de la Saire*’ which extends until a depth of 25 m (L.A.T) around Tatihou island (until 10 m depth L.A.T), at the ‘*Ben-être*’ beacon islet (0 m depths L.A.T) and south of Saint-Vaast-La-Hougue harbor (Figure 1, Main map). This is close to the oyster farms on the Brioverian rock outcrops. Sandy tidal flats are well developed in the central region and bounded by the coastline to the west and north, by oyster farms, toward the south, and by a slope break around the 0 m level (L.A.T) to the east. LiDAR analysis allows us to highlight five sedimentary structures (1–5 in Main map).

4.1.2. Channel networks

The channels and gullies of the Saire networks are well developed in the north (1 on Main map), established in a NW-SE direction, from the estuary to the ‘*pointe de la Saire*’ over 2 km. The fluvial system upstream can be classified as a ‘braided stream’ due to the presence of central banks separating the channels (Figure 2A). The north and central channels are V-shaped, they reach a maximum depth of 50 cm, and vary in width from 5 to 15 m. The river sides are symmetric with a mean slope of 6%. Channels are separated by central banks covered by well-developed tidal bars as highlighted on the A/B profile (Figure 2). The banks are topped from the south to the north by three and then two narrow (5 m wide) and thin (10–20 cm high) tidal bars. Upstream, the river is a system of meanders (Figure 2B). Central banks are rare, and terraces bound the main channel. The river channel is deeper (1 m) and forms meanders bordering alternatively on the north and south river banks. On the C-D profile (Figure 2), the main channel borders the north side and is steeper (5.9%) than the gently sloping south side (1.4%) where a terrace has developed. The terrace

is 50 m wide and raised 50 cm above the channel. In this part, the central channel is overlapped by bars characteristic of a tidal-dominated environment. A bar cuts the central channel on the C-D profile (Figure 2), separating the main channel into two sections: one dominated by the ebb and the other by the flood.

A smaller network of channels can be observed in the south of the study area (2 on Main map). Gullies cut the Brioverian outcrops before merging at the north of Tatihou Island. Networks are connected to the sea eastward, where the general slope of 0 meters (L.A.T) is developed. Gullies are shallow (20 cm) and narrow (5–10 m wide).

4.1.3. Marine dune field

The dune field covers an area of 194×10^3 m² (3 on Main map). It consists of 11 asymmetric dunes from 30 to 110 cm high and with a mean wavelength of 80 m (a to k on Figure 2C, Main map). Their sinuous crests are mainly oriented N-S. Dune asymmetry differs within the field. The biggest of six southern dunes (a, c, d, and f) have steep sides (mean slope of 2.3%) oriented toward the west, and gentle ones (mean slope of 0.6%) toward the east. The two others (b and e) present a reverse morphology to the five northern dunes (g to k) (Figure 2C, Main map).

4.1.4. Sandy prism

A sandy prism is present on the granite platform of the ‘*pointe de la Saire*’ and it extends 600 m, toward the west (4 in Main map) along the north coastline of Saire Bay. It is 50–110 m long and 0.4–1.20 m high. Its morphology is complex; it is topped by numerous sandy bars (9), eight are oriented according to the main direction (NW to SE), and one is oriented perpendicular (N-S).

4.1.5. Sand banks

Sand banks are spread over the entire study area but can be grouped according to their characteristics and location into two sets (5 and 6 in Main map). These structures are between 10–50 cm high, with variable length and width, but always symmetrical shape. They are oriented from south to north. The first set, ‘*Tatihou banks*’ (5 in Main map), includes five banks located to the north of Tatihou Island. They are oriented NE-SW with a mean length of 390 m and width of 25 m. Their crests are curved. The second set (6 in Main map, Figure 2E), ‘*Saire banks*’ is oriented similarly and located on both sides of the Saire river. They are located along the edge of the tidal flat (0 m L.A.T). They are also shorter (average of 170 m) and wider (average of 30 m). In contrast to the curved morphology of the first set, their crests are straight.

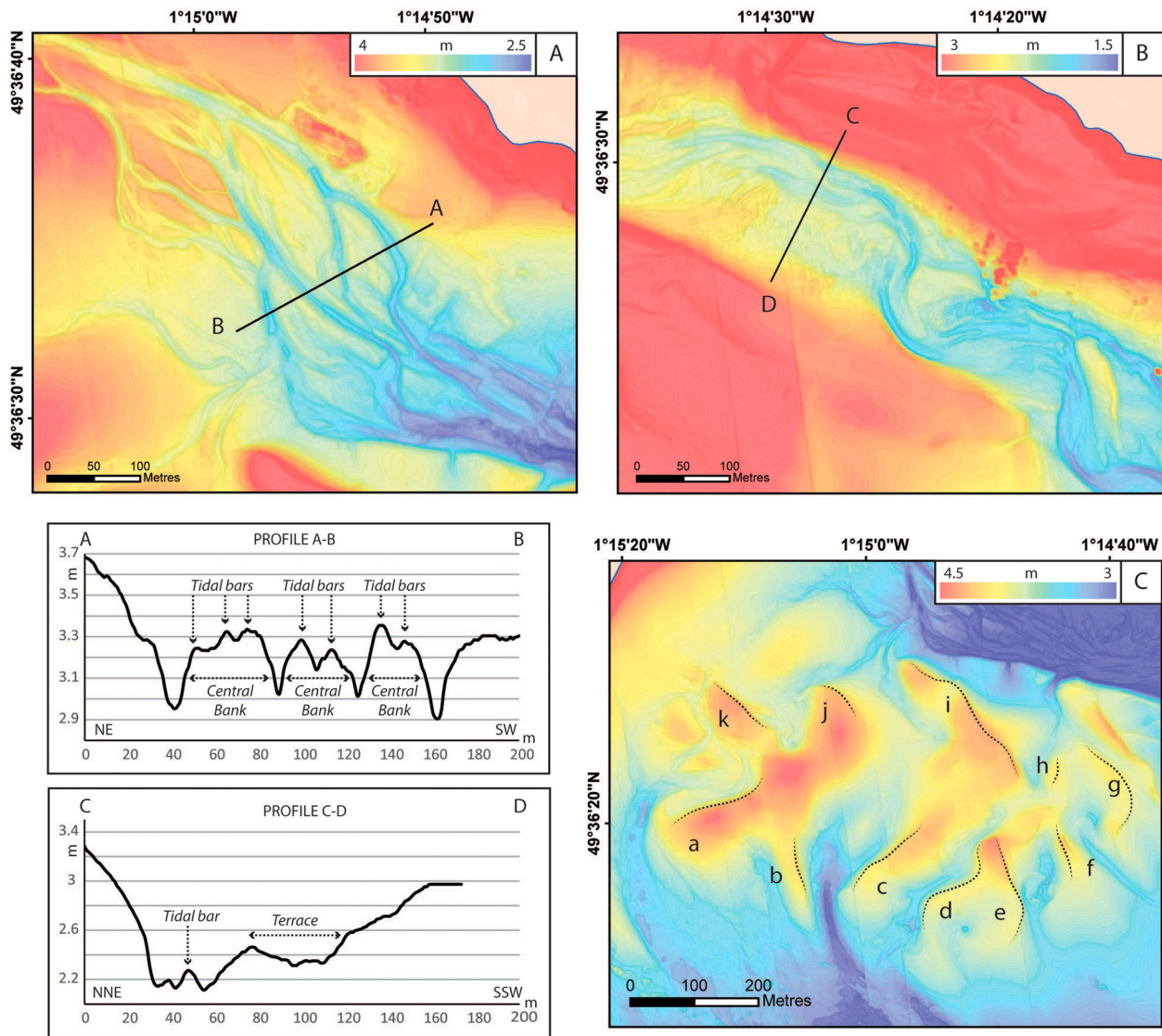


Figure 2. Sedimentary feature in the Saire Bay (numbers refer to the main map): A. Details of channel morphology in upstream (1) in main map, B. Details of channel morphology in downstream (1) in main map, C. Central dune field, letters a to k highlight the crests of each dune (3) in main map and channel morphology profiles A/B and C/D.

4.2. Sedimentological distribution

4.2.1. Grain-size results

To interpret grain size results, a PCA analysis was performed (Figure 3). Individual populations are made up of 200 sediment samples (Figure 3A), and the variables correspond to the seven grain-size classes described by Wentworth (1922) and modified by Blott and Pye (2001) (Figure 3B). PCA components 1 and 2 explain 78% of the variance. The variable vectors describe four sets, each displayed on a different quadrant in Figure 3B. Set 1, in the top left corner, is defined by coarse sand (CS, 500–1000 μm) and very coarse sand (VCS, 1000–2000 μm) (Figure 3B). Set 2, in the left bottom corner, is represented by medium sand (MS, 500–250 μm), and set 3, in the right bottom corner, by fine sand (FS, 125–250 μm). Set 4, in the right upper corner, includes finer grain-size from clay (0–4 μm) to very fine sand (VFS, 63–125 μm). The individual

population's distribution (Figure 3A) describes a 'V' shape, highlighting three clusters. Most populations are localized on the left side of the 'V', thus reflecting set 2's (Medium Sand) principal dominance in the samples. The spread on the left 'V' shape describes a gradient formed by two opposite clusters: from the coarse sand cluster (C1), associated to set 1, to the fine sand cluster (C2), associated to set 3. The right side of the 'V' is formed by only twenty samples (individual), distributed between C2 (fine sand) and C3 (mud). It forms a second gradient associated with a silting-up phenomenon.

Concentrated with an average of 16% in most parts of the tidal flat, the coarser set (set 1) is the main grain size type of the principal sedimentary structures of the sandy prism (40%, 3 in Main map), central dunes (25–35%, 1 in Main map) and northern bank (25–35%, 5 in Main map). Set 2 (250–500 μm) is almost ubiquitous (concentrated between 30 and 50% except in the Saire estuary) on the entire sandy tidal flat. It is

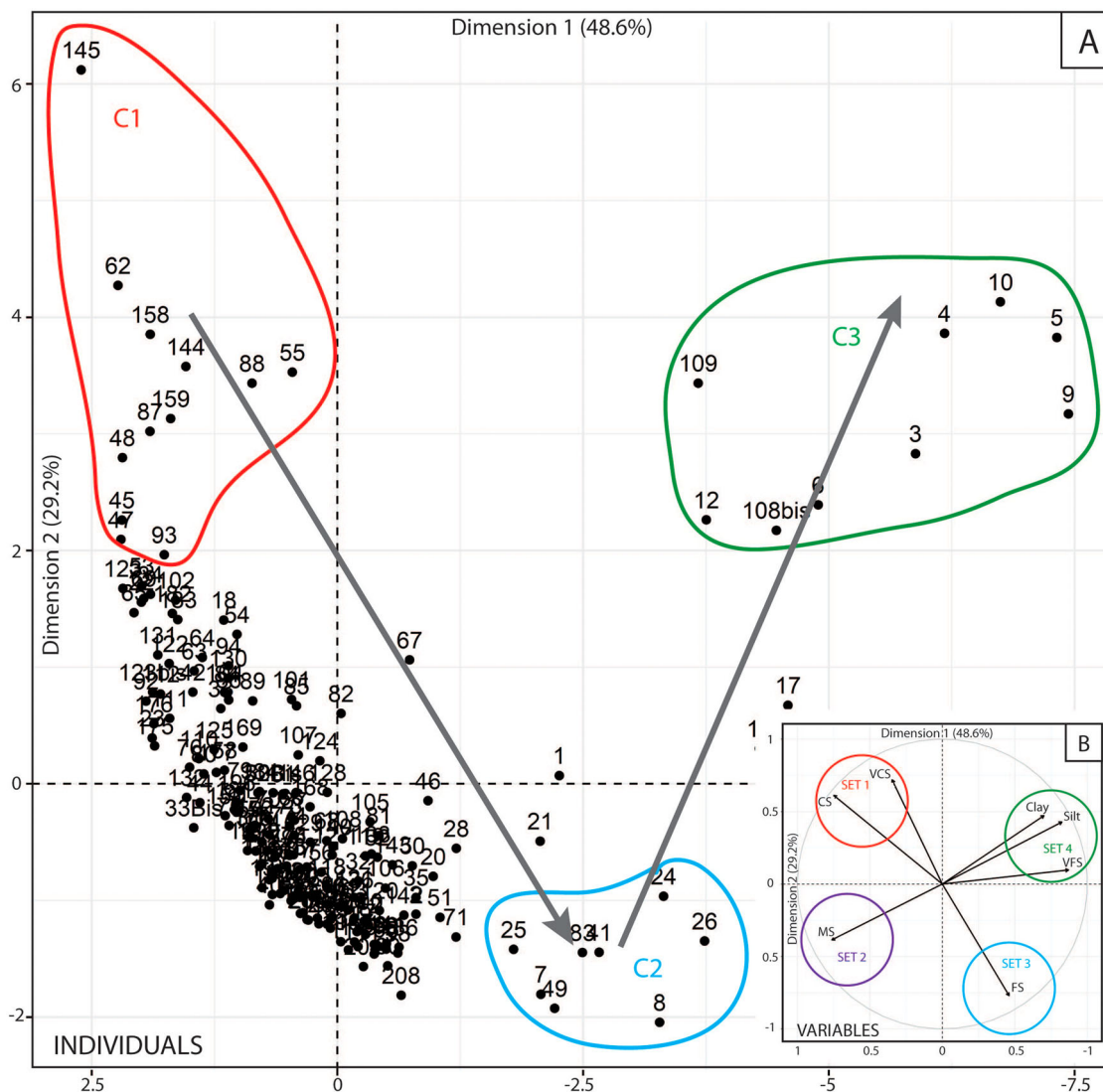


Figure 3. PCA results of grain-size analysis. A. Dispersion of individuals and organized in 3 clusters and B. Dispersion of variable and organized in 4 sets.

however more concentrated at the east of limit (α) defined by a line parallel to the ‘longue rive’ dyke and linking the Brioverian outcrops to the ‘Jonville beach’ through the central dunes (sets 1–4 in Main map). The fine sand set (set 3; 125–250 μm) is well represented (average of 20%), except in proximity to the limit (α) (< 16%). Its repartition is heterogenous. At the western part, at the south of the Saire estuary, set 3 is highly concentrated and constitutes more than 50% of sediment. From this, two decreasing grain size gradients can be described: one from the patch to the S, along the coastline, and a second to the SE. The muddy/very fine sand grain size-fraction (set 4; < 125 μm) is poorly represented in the study area with an average percentage of < 10%. This fraction is mainly located at the Saire estuary where it reaches a very high concentration (>50%). This muddy patch covers the north side of the estuary. At downstream in the channel, muddy sediments quickly disappear in favor of sandy sediment (Main map).

4.2.2. Geochemistry results

The statistical analysis of geochemistry results allows to select five chemical elements as being the most representative of the sediment sources: Calcium (Ca), Strontium (Sr), Manganese (Mn), and Titanium (Ti). A fifth element, Silicon (Si), normally very concentrated in terrestrial sediments, was chosen to construct the PCA (Principal Component Analysis) but it will not be used here for source description. Silicon is a quartz tracer and despite the terrigenous primal source of quartz, an unknown proportion of this mineral could be delivered to the Bay of Saire area by marine hydrodynamics. Geochemistry PCA components (1 and 2) represent a total variability of 88% (Figure 4A). Variables are organized into two sets (Figure 4B). To the left, set 1 shows Ca and Sr (Spearman correlation (ρ) is about 0.78, Table 2) and in the upper right corner, set 2 shows associated Mn and Ti (Spearman correlation (ρ) is about 0.73, Table 2). Individuals spread between these two sets and form a

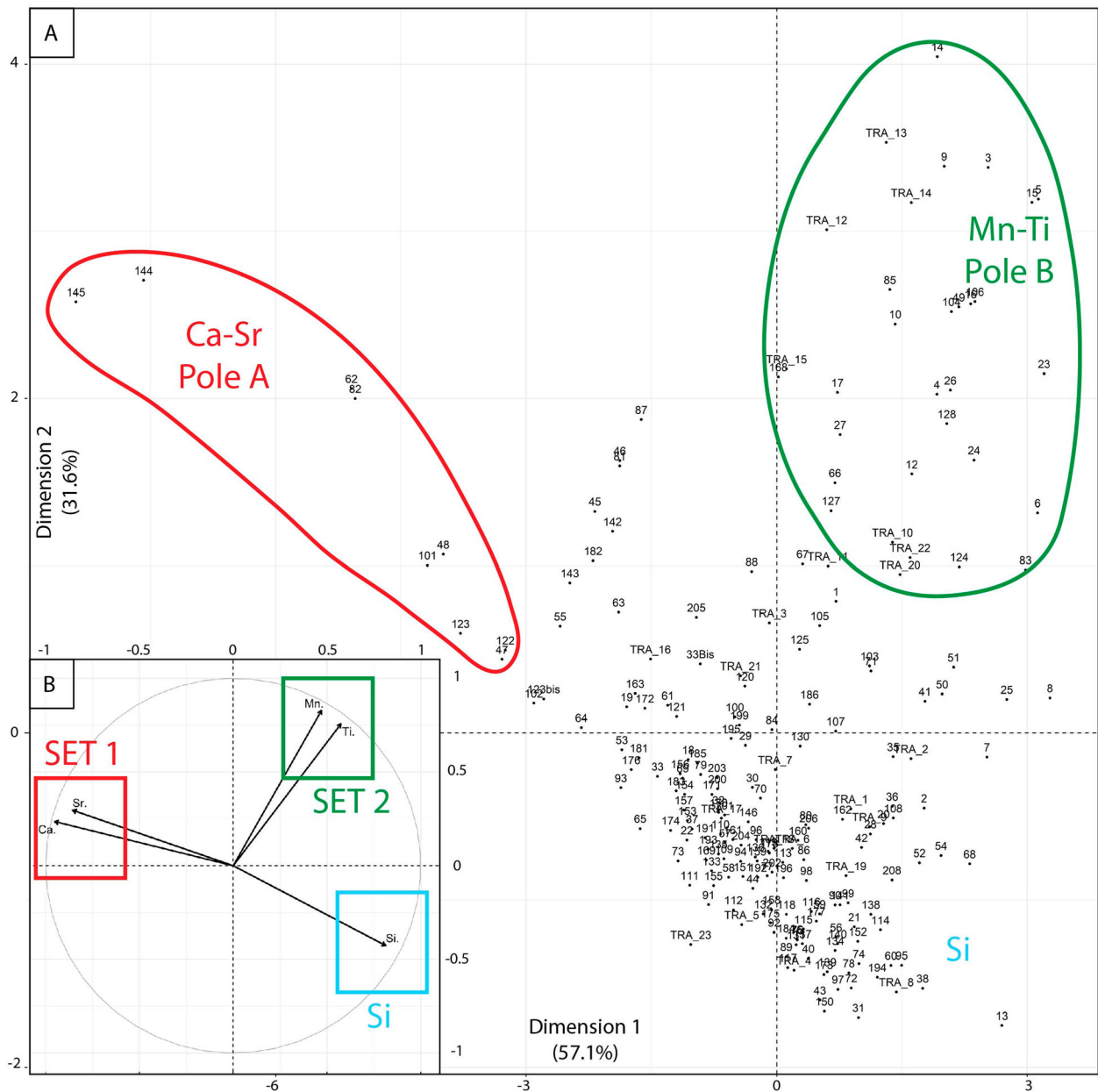


Figure 4. PCA results of chemical element content: A. Dispersion of individuals, organized in two sets, and B. variables, organized in two poles Ca-Sr and Mn-Ti. .

‘triangle’ shape where each angle can be associated with two poles (A and B, Figure 4A) and Si.

Pole A (Ca-Sr) represents chemical elements mostly concentrated in marine carbonates, interpreted here as the marker of marine sources (shell debris or fragments) (Baux et al., 2017). Samples forming pole A are mainly located on the top of the main morphologic structures of the study area, such as the sandy prism (27% of Ca concentration), banks, and dunes (20% Ca concentration) and mainly for the southernmost banks (Ca set 1, Main map).

Pole B consists of samples located at the Saire estuary. Analyses performed on the Saire watershed (Table 1) show that fluvial sediments are enriched with Ti and Mn, both chemical elements forming pole B. It is therefore a marker of the finer continental sediment source. Sediments contained in this pole probably

come from the erosion of brioverian rocks forming the basement of the Saire watershed. Points in the center of the ‘triangle’ shape described by poles A, B and Si are indicative of a combination of the two sources (Figure 4).

4.2.3. Comparison of grain-size and geochemistry results

Table 2 shows the Spearman correlation between particle size (studied classes) and the four geochemical elements highlighted by PCA analysis. The maximum value obtained highlights the correlation between very fine and muddy sediment and Ti (0.71) and Mn (0.63). This confirms that very fine sediments are brought by the Saire river and trapped in the estuary by tidal and fluvial currents. Spearman correlations between Ca-Sr and coarse sand and gravels (set 1), are about 0.51 and

Table 2. Spearman correlation results between grain-size sets and chemical elements.

	Ca	Sr	Ti	Mn
Set 1 ($> 500 \mu\text{m}$)	0.51	0.44	-0.46	-0.36
Set 2 ($500\text{--}250 \mu\text{m}$)	0.24	0.12	-0.64	-0.55
Set 3 ($250\text{--}125 \mu\text{m}$)	-0.44	-0.43	0.29	0.21
Set 4 ($< 125 \mu\text{m}$)	-0.39	-0.28	0.71	0.63

0.44, respectively. They allow us to connect the marine sediment source (shell fragments) with the coarser grain-size fractions ($>500 \mu\text{m}$).

4.3. Hydrodynamics of the bay

The integration of morphological, geochemical, and sedimentological data makes it possible to identify six sectors (A to F, Figure 5) with sedimentary hydrodynamics specific to each of them and interpreted within the hydrodynamic scheme.

The Saire River is isolated from the intertidal area during high tide by a floodgate where fluvial inputs (water and sediments) accumulate. During the ebb, pressure exercised by accumulated fluvial water is responsible for the floodgate opening. Sediments are

thus rapidly evacuated ($< 125 \mu\text{m}$ and Ti-Mn enriched) (Figure 5, sector A). Fine sediments exported to the sea can be divided into two paths. The first path follows the 'longue rive' dyke towards the SSW first and then moves towards the Brioverian depression according to the NW-SE direction along the oyster farms (Figure 5, sector B). A second path interweaves with the Saire channel (Figure 5, sector C). During the flood tide, fine sediments silt up mainly in the bay bottom (Figure 5, sector A) where they are trapped at the north of the estuary. This occurs during the flood tide, where fine sediments deposited during slack water are resuspended and redeposited in the boundary area between the fluvial and tidal currents. Thus, discharges linked to the tide follow two channeled areas (Figure 5, sectors B and C): the Saire channel at the north and the brioverian depression at the south. While less visible in morphology, the south depression (Figure 5, sector B), devoid of sedimentary cover it is considered to be the main vector of sediment transport.

Swell action is visible thanks to the sandy banks located in the external part of the bay (Main map 3, 4 et 5) (Figure 5, sector E). Swell energy, dissipated by the east slope break (0 L.A.T), generates turbulence when it reaches the rocky outcrops. Coarse sediments are produced by their erosion and then quickly

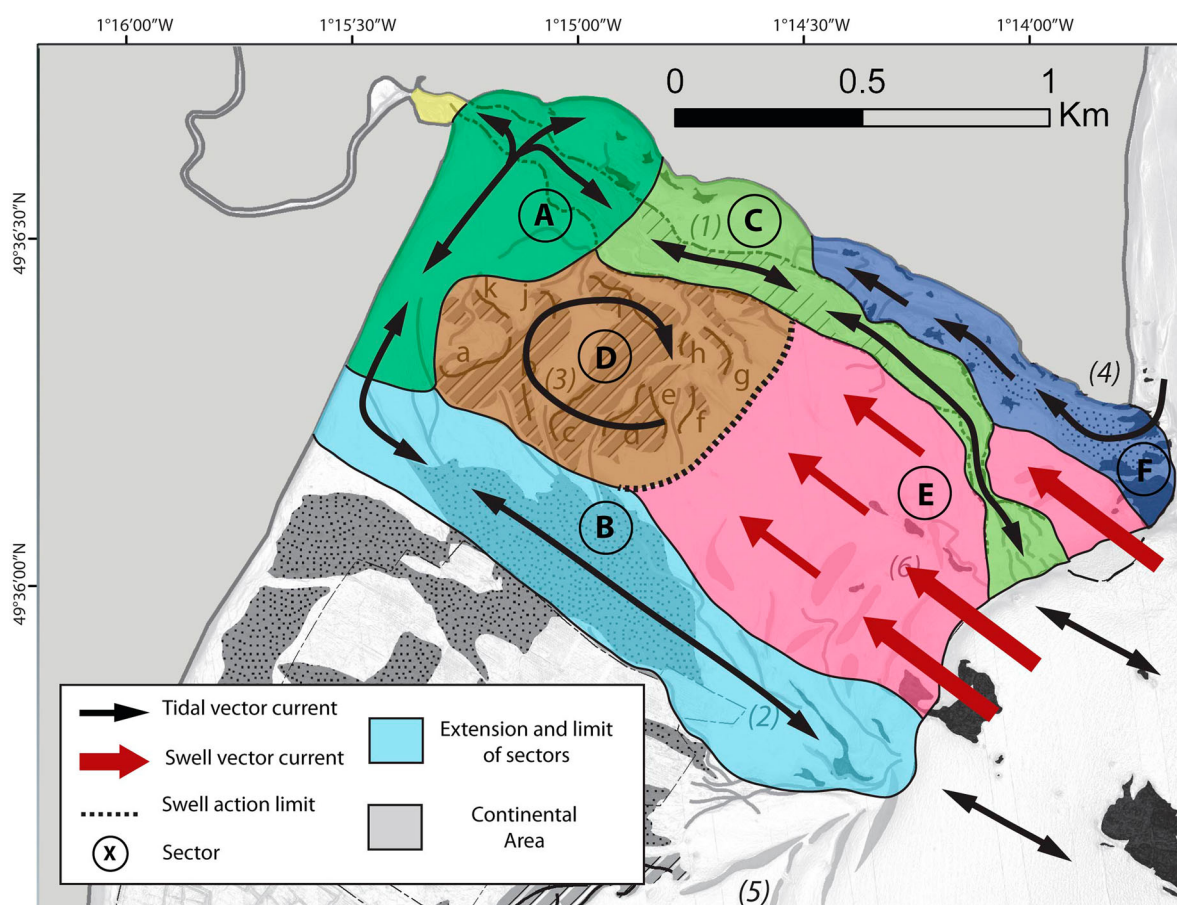


Figure 5. Schematic representation of sedimentary transport superimposed on morphology (Main map). Sectors (A to F) are represented by different colors. Black arrows represent the tidal orientation transport.

deposited nearby. Swells, associated with tidal current and coastal morphology, reach a maximum along the north littoral zone at the ‘*pointe de la Saire*’. Due to the Venturi effect, a shelly sandy prism is created from the granitic platform (Figure 5, sector F). Littoral drift takes place up to the ‘*Jonville beach*’ cob.

The central dune field forms due to its location (Figure 5, sector D). Indeed, alternative fluvial and tidal currents in sectors B and C (Figure 5) can explain medium and coarse sandy accumulations. Dunes are fed during each tide by shelly coarse sand coming from various gullies. They are forced by swells impacting the western part, downstream of the (α) limit (Main map).

It appears that the overall dynamics of the bay result from the interactions between the flows linked to the fluvial inputs and those linked to the tide, the swell only influencing the outermost part, and limited to the east by the (α) limit (sector E) for two reasons: (1) Central dunes (sector D) attenuate the swell during flood tides. At high tide, the water depth is too high for that swell to be impacted. (2) The depression along the ‘*longue rive*’ dyke (sector A) structure, which is maintained by strong tidal currents running into the bay by the brioverian depression (sector B).

5. Conclusions

Morphological study (LiDAR data) coupled with a field approach based on grain-size and geochemistry statistical analysis allows us to highlight the complex circulation of sediment in this sandy tidal flat. The superficial cover is governed by hydrodynamics mainly dominated by tidal currents. It is, however, locally impacted by swells and fluvial currents. Fluvial energy, impacting mainly the eastern part, is rapidly dissipated to the benefit of tidal currents. Swells act only on the western part mainly dissipated by the slope break, the central dune, and the depression before the ‘*longue rive*’ dyke. Contrary to what is generally expected in estuary sediment interactions and exchanges between land and sea are not accomplished by the impression of the main channel observed at the north of the bay in continuity with the main river (Saire). Exchanges happen south and are characterized by a shallower channel of very energetic currents that are accelerated due to their location: wedged between a rocky outcrop at the south and by the central tidal flat of the bay to the north. This is induced by anthropogenic constructions including an oyster farm to the south, the ‘*longue rive*’ dyke to the east, and several groynes perpendicular to the coastline to the north.

Further studies are underway to compare this morpho-sedimentologic scheme with modelling results. New morphological data are currently being acquired and analyzed with the aim of better characterizing the

evolution of the Saire Bay and better predicting flooding and erosion events.

Acknowledgements

We would like to thank the SHOM, IGN, and ROLNP for providing the LIDAR data (litto3D©). We are also grateful to the team of people who participated in this research project: Anne Duperret, Régis Gallon, Henri Gandois, Martin Protat, Cyril Marcigny, and Pierre Stephan. Katalin Kovacs post-edited the English for style and grammar.

Disclosure statement

No potential conflict of interest was reported by the authors.

Funding

Data were obtained through the scientific project « Etudes environnementales archéologiques et contemporaines de l'estuaire de la Saire à l'île de Tatihou » funded by the ROLNP (Réseau d'Observation du Littoral Normand Picard).

Software

Software ©QGIS 3.10 (A Coruna) was used to create the bathymetric map and sedimentological data maps. Map layout and final editing were performed using ©Adobe Illustrator CS 6. PCA were produced thanks to ©RStudio software.

Data availability statement

The data that support the findings of this study are openly available in website of the coastal observation network named ‘ROLNP’ (Réseau d'Observation du littoral de Normandie et des Hauts-de-France) at <https://rolnp.fr/rolnp/>, reference number <https://rolnp.fr/rolnp/index.php/176-ressources-et-travaux/strategie-de-suivi/865-appel-a-projets-ii-analyse-des-donnees-lidar-de-la-strategie-de-suivi-du-littoral#projet-iv>.

Geolocation information

Our study area is located in the region of Normandy in France. Saire Bay is developed in the eastern part of the Cotentin peninsula at coordinates: 49.602,045,5012849°, -1.2447492309870871°.

ORCID

Gregoire Gwendoline  <http://orcid.org/0000-0003-3369-8639>

References

Allen, J. R. L. (2000). Morphodynamics of Holocene salt marshes: A review sketch from the Atlantic and southern

- North Sea coasts of Europe. *Quaternary Science Reviews*, 19(12), 1155–1231. doi:10.1016/S0277-3791(99)00034-7.
- Audère, M., & Robin, M. (2021). Assessment of the vulnerability of sandy coasts to erosion (short and medium term) for coastal risk mapping (Vendée, W France). *Ocean & Coastal Management*, 201, 105452. <https://doi.org/10.1016/j.ocecoaman.2020.105452>
- Baux, N., Murat, A., Poizot, E., Méar, Y., Gregoire, G., Lesourd, S., & Dauvin, J. C. (2022). An innovative geostatistical sediment trend analysis using geochemical data to highlight sediment sources and transport. *Computational Geosciences*, 26(2), 263–278. doi:10.1007/s10596-021-10123-5
- Baux, N., Pezy, J. P., Bachelet, Q., Baffreau, A., Méar, Y., Poizot, E., Guyonnet, B., & Dauvin, J. C. (2017). Soft bottom macrobenthic communities in a semi-enclosed Bay bordering the English channel: The Rade de Cherbourg. *Regional Studies in Marine Science*, 9, 106–116. <https://doi.org/10.1016/j.rsma.2016.11.010>
- Blott, S. J., & Pye, K. (2001). GRADISTAT: A grain size distribution and statistics package for the analysis of unconsolidated sediments. *Earth Surface Processes and Landforms*, 26(11), 1237–1248. doi:10.1002/esp.261
- Castelle, B., Marieu, V., Bujan, S., Splinter, K. D., Robinet, A., Sénéchal, N., & Ferreira, S. (2015). Impact of the winter 2013–2014 series of severe Western Europe storms on a double-barred sandy coast: Beach and dune erosion and megacusp embayments. *Geomorphology*, 238, 135–148. <https://doi.org/10.1016/j.geomorph.2015.03.006>
- Costa, S., Maquaire, O., Letortu, P., Thirard, G., Compain, V., Roulland, T., Medjkane, M., Davidson, R., Graff, K., Lissak, C., Delacourt, C., Duguet, T., Fauchard, C., & Antoine, R. (2019). Sedimentary coastal cliffs of normandy: Modalities and quantification of retreat. *Journal of Coastal Research*, 88(SI), 46–60. <https://doi.org/10.2112/SI88-005.1>
- Davis, R. A., & Balson, P. S. (1992). Stratigraphy of a North Sea tidal sand ridge. *Journal of Sedimentary Research*, 62(1), 116–121. <https://doi.org/10.1306/D42678A2-2B26-11D7-8648000102C1865D>
- Day, J. W., Agboola, J., Chen, Z., D'Elia, C., Forbes, D. L., Giosan, L., Kemp, P., Kuenzer, C., Lane, R. R., Ramachandran, R., Syvitski, J., & Yanez-Arancibia, A. (2016). Approaches to defining deltaic sustainability in the 21st century. *Estuarine, Coastal and Shelf Science*, 183, 275–291. <https://doi.org/10.1016/j.ecss.2016.06.018>
- DDTM (Direction Départementale des Territoires et de la mer de la Manche). (2016). Plan de prévention des risques littoraux des communes de Réville, Saint-Vaast-la-Hougue et Quettehou. 40 p. <https://www.manche.gouv.fr/Actions-de-l-Etat/Environnement-risques-naturels-et-technologiques/Risques-Naturels-et-Technologiques/Plans-de-prevention-des-risques/Plans-de-Prevention-des-Risques-naturels-PPRN/PPRN-approuves-en-vigueur/Plans-de-Prevention-des-Risques-Littoraux-PPRL/PPRL-de-Saint-Vaast-la-Hougue-Quettehou-et-Reville>
- Dissler, E. (1987). *Evolution géodynamique cadomienne du Nord-Cotentin (Massif armoricain)* (Thèse de doctorat). Université de Caen. <https://www.theses.fr/1987CAEN2048>
- Du, J., Shen, J., Zhang, Y. J., Ye, F., Liu, Z., Wang, Z., & ... Wang, H. V. (2018). Tidal response to sea-level rise in different types of estuaries: The importance of length, bathymetry, and geometry. *Geophysical Research Letters*, 45(1), 227–235. <https://doi.org/10.1002/2017GL075963>
- Dyer, K. R., & Huntley, D. A. (1999). The origin, classification and modelling of sand banks and ridges. *Continental Shelf Research*, 19(10), 1285–1330. [https://doi.org/10.1016/S0278-4343\(99\)00028-X](https://doi.org/10.1016/S0278-4343(99)00028-X)
- FitzGerald, D. M., Fenster, M. S., Argow, B. A., & Buynevich, I. V. (2008). Coastal impacts due to sea-level rise. *Annual Review of Earth and Planetary Sciences*, 36(1), 601–647. doi:10.1146/annurev.earth.35.031306.140139
- Foteinis, S., & Synolakis, C. E. (2015). Beach erosion threatens minoan beaches: A case study of coastal retreat in crete. *Shore & Beach*, 83(1), 53–62. https://www.academia.edu/download/44666318/FoteinisSpring2015_83_1-4.pdf
- Garlan, T. (2007). Study on Marine Sandwave dynamics. *The International Hydrographic Review*, 8(1), 26–37. <https://journals.lib.unb.ca/index.php/ihr/article/view/20779>
- Garlan, T., Marches, E., & Brenon, E. (2015). A classification of scouring marks in macrotidal environments from analysis of long-term wreck marks. In *The Proceedings of the Coastal Sediments 2015*, 14 p., https://doi.org/10.1142/9789814689977_0202
- Graindor, M. J., & Wasserburg, G. J. (1962). Déterminations d'âges absolus dans le nord du Massif armoricain. *Comptes Rendus Hebdomadaires des Séances de l'Académie des Sciences*, 254(22), 3875–3877.
- Gresselin, F. (1990). *Evolution varisque du massif armoricain oriental: Insertion dans une transversale ouest-européenne* (Thèse de doctorat). Université de Caen. 355 p. <https://www.theses.fr/1990CAEN2049>
- IPCC. (2019). Summary for Policymakers. In: IPCC Special Report on the Ocean and Cryosphere in a Changing Climate [H.- O. Pörtner, D.C. Roberts, V. Masson-Delmotte, P. Zhai, M. Tignor, E. Poloczanska, K. Mintenbeck, M. Nicolai, A. Okem, J. Petzold, B. Rama, N. Weyer (eds.)]. chrome-extension://efaidnbmnnnibpcajpcgclefindmkaj/https://www.ipcc.ch/site/assets/uploads/sites/3/2019/12/SROCC_FullReport_FINAL.pdf
- IPCC. (2021). Climate change 2021: the physical science basis. contribution of working group I to the sixth assessment report of the intergovernmental panel on climate change [Masson-Delmotte V, Zhai P, Pirani A, Connors SL, Péan C, Berger S, Caud N, Chen Y, Goldfarb L, Gomis MI, Huang M, Leitzell K, Lonnoy E, Matthews JBR, Maycock TK, Waterfield T, Yelekçi O, Yu R, Zhou B (eds)]. Cambridge University Press. chrome-extension://efaidnbmnnnibpcajpcgclefindmkaj/https://www.ipcc.ch/report/ar6/wg1/downloads/report/IPCC_AR6_WGI_SPM_final.pdf
- Isla, F. I., Cortizo, L., Merlotto, A., Bértola, G., Albisetti, M. P., & Finocchietti, C. (2018). Erosion in Buenos Aires province: Coastal-management policy revisited. *Ocean & Coastal Management*, 156, 107–116. <https://doi.org/10.1016/j.ocecoaman.2017.09.008>
- Le Bot, S. (2001). Morphodynamique de dunes sous-marines sous influence des marées et des tempêtes: processus hydro-sédimentaires et enregistrement : exemple du Pas-de-Calais. Thèse de doctorat Université de Lille 1, 272 p.
- Le Cam, H., & Baraer, F. (2012). Climatologie marine. Sous-région marine Manche-Mer du Nord. Evaluation Initiale DCsMM. https://www.ifremer.fr/sextant_doc/dcsmm/documents/Evaluation_initiale/MMN/EE/MMN_EE_01_Climatologie_marine
- Leroux, J. (1897). Petite histoire de Saint-Vaast-la-Hougue. *EDR*, 1897, 207–211. <https://gallica.bnf.fr/ark:/12148/bpt6k143458z.texteImage>
- Luijendijk, A., Hagenaars, G., Ranasinghe, R., Baart, F., Donchyts, G., & Aarninkhof, S. (2018). The state of the world's beaches. *Scientific Reports*, 8(1), 1–11. <https://doi.org/10.1038/s41598-018-24630-6>

- Neill, S. P., Scourse, J. D., Bigg, G. R., & Uehara, K. (2009). Changes in wave climate over the northwest European shelf seas during the last 12,000 years. *Journal of Geophysical Research: Oceans*, 114(n°C6), 19 p. <https://doi.org/10.1029/2009JC005288>
- Pommepuy, M., Le Guyader, S., Le Saux, J. C., Caprais, M. P., Riou, P., Le Goff, R., Dumas, F., Pothier, P., Bon, F., Kohli, E., Poncet, D., Cohen, J., & Libersou, S. (2005). Etude pour la reconquête de la qualité des eaux littorales et de la salubrité des coquillages dans le secteur de production conchylicole Cul de Loup – Lestre. IFREMER, CHU Dijon, INRA, 119 p.
- R Core Team. (2016). *R: A language and environment for statistical computing*. R Foundation for Statistical Computing. URL <http://www.R-project.org/>
- Roulland, T., Maquaire, O., Costa, S., Medjkane, M., Davidson, R., Fauchard, C., & Antoine, R. (2022). Seasonal activity quantification of coast badlands by TLS monitoring over five years at the “vaches noires” cliffs (normandy, France). *Geomorphology*, 400, 37–55. <https://doi.org/10.1016/j.geomorph.2021.108083>.
- Savini, J.-R. (2021). - 250012324, Anse du Cul de Loup. - INPN, SPN-MNHN Paris, 46 p. <https://inpn.mnhn.fr/zone/znieff/250012324/tab/commentaires>
- SHOM. (1996). Atlas des courants de marée – baie de seine. *De Cherbourg, à Fécamp*, 561-UJC.
- Tessier, B. (2012). Stratigraphy of tide-dominated estuaries. *Principles of Tidal Sedimentology*, 109–128. https://doi.org/10.1007/978-94-007-0123-6_6
- Wentworth, C. K. (1922). A scale of grade and class terms for clastic sediments. *The Journal of Geology*, 30(5), 377–392. <https://doi.org/10.1086/622910>
- Williams, S. J. (2013). Sea-level rise implications for coastal regions. *Journal of Coastal Research*, 63, 184–196. <https://doi.org/10.2112/SI63-015.1>